Chapter 2
Proposal for Demonstrating the Hong–Ou–Mandel Effect with Matter Waves

Two-particle interference is a quintessential effect of quantum mechanics which is perhaps most beautifully demonstrated by the Hong–Ou–Mandel effect. In this phenomenon, the probability amplitudes of two indistinguishable photons entering opposing inputs of a beam-splitter interfere destructively, in a manner which is not describable by any classical theory. When realized with photons prepared in the two-mode squeezed vacuum state [1], this two-particle interference also serves as a demonstration of the strong non-classical correlations between the modes, in particular a violation of the Cauchy–Schwarz inequality. This elegant effect is thus intrinsically related to a violation of a Bell inequality, as both phenomena rely on underlying non-classical features of the quantum state.

In this chapter we outline a proposal to demonstrate the effect with massive particles, utilizing pairs of atoms produced by spontaneous four-wave mixing via colliding condensates, which, as demonstrated in Sect. 1.4.2, reduces in the simplest model to the same two-mode squeezed vacuum state. However, unlike the two-mode quantum optics scheme, the multimode nature of the collision halo motivates us to formulate a new measurement protocol to quantify the effect in the atomic case. An experimental demonstration of the effect has a two-fold impact for future tests of a Bell inequality in this system. Firstly, the interferometric scheme required for the Hong–Ou–Mandel effect, comprising of a series of laser-induced Bragg pulses (the atom-optics analogs of mirrors and beam-splitters), is strongly related to the Rarity–Tapster setup employed in Chap. 3 and thus acts as a stepping-stone for any experimental proposal involving atom-optics mirrors and beam-splitters. Secondly, as discussed above, a true demonstration of the effect requires an interference visibility of more than 50 % (relative to the background level of distinguishable paths through the beam-splitter) which is equivalent to a violation of the classical Cauchy–Schwarz inequality. Such non-classical correlations are a pre-requisite for a violation of a Bell inequality.

R.J. Lewis-Swan, *Ultracold Atoms for Foundational Tests of Quantum Mechanics*, Springer Theses, DOI 10.1007/978-3-319-41048-7_2

The remainder of this chapter is adapted from the published article: *'Proposal for demonstrating the Hong–Ou–Mandel effect with matter waves'* [R.J. Lewis-Swan and K.V. Kheruntsyan, Nature Comm. **5**, 3752 (2013)]. The supplementary information of this article can be found in Appendix C.

2.1 Introduction

Since its first demonstration, the Hong–Ou–Mandel (HOM) effect [1] has become a textbook example of quantum mechanical two-particle interference using pairs of indistinguishable photons. When two such photons enter a 50:50 beam splitter, with one photon in each input port, they both preferentially exit from the same output port, even though each photon individually had a 50:50 chance of exiting through either output port. The HOM effect was first demonstrated using optical parametric down-conversion [1]; the same setup, but with an addition of linear polarisers, was subsequently used to demonstrate a violation of a Bell inequality [2] which is of fundamental importance to validating some of the foundational principles of quantum mechanics such as quantum nonlocality and long-distance entanglement.

The HOM effect is a result of destructive quantum interference in a (bosonic) twin-photon state, which leads to a characteristic dip in the photon coincidence counts at two photodetectors placed at the output ports of a beam splitter. The destructive interference occurs between two *indistinguishable* paths corresponding to the photons being both reflected from, or both transmitted through, the beam splitter. Apart from being of fundamental importance to quantum physics, the HOM effect underlies the basic entangling mechanism in linear optical quantum computing [3], in which a twin-photon state $|1, 1\rangle$ is converted into a quantum superposition $\frac{1}{\sqrt{2}}(|2, 0\rangle - |0, 2\rangle)$—the simplest example of the elusive 'NOON' state [4]. Whereas the HOM effect with (massless) photons has been extensively studied in quantum optics (see [5, 6] and references therein), two-particle quantum interference with massive particles remains largely unexplored. A matter wave demonstration of the HOM effect would be a major advance in experimental quantum physics, enabling an expansion of foundational tests of quantum mechanics into previously unexplored regimes.

Here we propose an experiment which can realise the HOM effect with matter waves using a collision of two atomic Bose–Einstein condensates (BECs) (as in Refs. [7–11]) and a sequence of laser-induced Bragg pulses. The HOM interferometer uses pair-correlated atoms from the scattering halo that is generated during the collision through the process of spontaneous four-wave mixing. The pair-correlated atoms are being mixed with a sequence of two Bragg pulses [12, 13] in analogy with the use of twin-photons from parametric down conversion in the optical HOM scheme. The HOM effect is quantified via the measurement of a set of atom-atom pair correlation functions between the output ports of the interferometer. Using stochastic quantum simulations of the collisional dynamics and the sequence of Bragg pulses,

we predict a HOM-dip visibility of ∼69 % for realistic experimental parameters. A visibility larger than ∼50 % is indicative of stronger than classical correlations between the atoms in the scattering halo [10, 11, 14–16], which in turn renders our system as a suitable platform for demonstrating a Bell's inequality violation with matter waves using a closely related Rarity–Tapster scheme [17].

2.2 Setup

The schematic diagram of the proposed experiment is shown in Fig. 2.1. A highly elongated (along the x-axis) BEC is initially split into two equal and counterpropagating halves traveling with momenta $\pm\mathbf{k}_0$ along z in the centre-of-mass frame. Constituent atoms undergo binary elastic collisions which produce a nearly spherical s-wave scattering halo of radius $k_r \simeq 0.95|\mathbf{k}_0|$ [9] in momentum space due to energy and momentum conservation. The elongated condensates have a disk shaped density distribution in momentum space, shown in Fig. 2.1b on the north and south poles of the halo. After the end of the collision (which in this geometry corresponds to complete spatial separation of the condensates in position space) we apply two counterpropagating lasers along the x-axis whose intensity and frequency are tuned to act as a resonant Bragg π-pulse with respect to two diametrically opposing momentum modes, $\mathbf{k}_1$ and $\mathbf{k}_2 = -\mathbf{k}_1$, situated on the equatorial plane of the halo and satisfying $|\mathbf{k}_{1,2}| = k_r$.

Previous experiments and theoretical work [7, 8, 10, 11, 18–23] have shown the existence of strong atom-atom correlation between such diametrically opposite modes, similar to the correlation between twin-photons in parametric down conver-

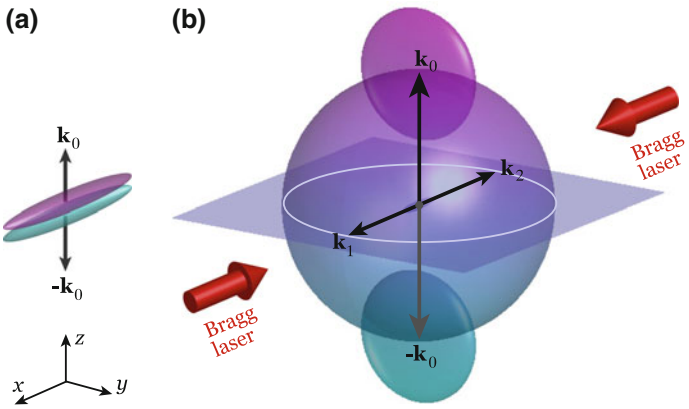

Fig. 2.1 **a** Schematic diagram of the geometry of collision of two elongated Bose–Einstein condensates in position space. **b** Momentum space distribution of the atomic cloud showing the (*disk shaped*) colliding condensates on the north and south poles of the spherical halo of scattered atoms (see text for further details)

sion. Applying the Bragg π-pulse to the collisional halo replicates an optical mirror and reverses the trajectories of the scattered atoms with momenta $\mathbf{k}_1$ and $\mathbf{k}_2$, and a finite region around them. We assume that the pulse is tuned to operate in the so-called Bragg regime of the Kapitza–Dirac effect [13, 24] (diffraction of a matter-wave from a standing light field), corresponding to conditions in which second- and higher-order diffractions are suppressed. The system is then allowed to propagate freely for a duration so that the targeted atomic wave-packets regain spatial overlap in position space. We then apply a second Bragg pulse—a $\pi/2$-pulse—to replicate an optical 50:50 beam-splitter, which is again targeted to couple $\mathbf{k}_1$ and $\mathbf{k}_2$, thus realising the HOM interferometer.

The timeline of the proposed experiment is illustrated in Fig. 2.2a, whereas the results of numerical simulations (see Methods) of the collision dynamics and the application of Bragg pulses are shown in Fig. 2.2b–d: (b) shows the equatorial slice of the momentum-space density distribution $n(\mathbf{k}, t)$ of the scattering halo at the end of collision; (c) and (d) show the halo density after the application of the π and $\pi/2$ pulses, respectively. The 'banana' shaped regions in (c) correspond to 'kicked' populations between the targeted momenta around $\mathbf{k}_1$ and $\mathbf{k}_2$ in the original scattering

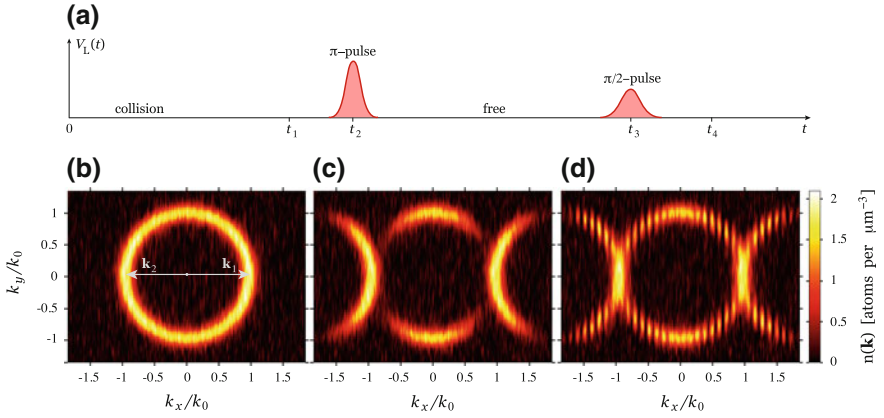

Fig. 2.2 **a**—Timeline of the proposed experiment; **b**–**d**—the results of numerical simulations showing the momentum-space density distribution $n(\mathbf{k})$ of scattered atoms on the equatorial plane of the halo. In panel (**a**), $V_L(t)$ denotes the depth of the lattice potential formed by the Bragg lasers, with the first hump indicating the mirror (π) pulse, while the second hump—the beam-splitter ($\pi/2$) pulse (the initial source-splitting pulse that sets up the collision of condensates is not shown for clarity). Panel (**b**) shows the density distribution after the collision, at $t_1 = 65\,\mu$s; **c**—after the π-pulse, centred at $t_2 = 75\,\mu$s and having a duration of $\tau_\pi = 2.5\,\mu$s (rms width of Gaussian envelope); and **d**—after the final $\pi/2$ pulse, with $\Delta t_{\text{free}} = t_3 - t_2 = 85\,\mu$s and $\tau_{\pi/2} = 2.5\,\mu$s (see Methods for further details; the durations shown on the time axis are not to scale). The momentum axes $k_{x,y}$ in panels (**b**)–(**d**) are normalised to the collision momentum $k_0 \equiv |\mathbf{k_0}|$ (in wave-number units), which in our simulations was $k_0 = 4.7 \times 10^6\,\text{m}^{-1}$. The simulations were carried out for an initial BEC containing a total of $N = 4.7 \times 10^4$ atoms of metastable helium (^{4}He*), prepared in a harmonic trap of frequencies $(\omega_x, \omega_y, \omega_z)/2\pi = (64, 1150, 1150)$ Hz, and colliding with the scattering length of $a = 5.3$ nm; all these parameters are very close to those realised in recent experiments [9, 10]

halo, while (d) shows the density distribution after mixing. The density modulation in (c) is simply the result of interference between the residual and transferred atomic populations after the π-pulse upon their recombination on the beamsplitter. The residual population is due to the fact that the pairs of off-resonance modes in these parts of the halo (which are coupled by the same Bragg pulses as they share the same momentum difference $2k_r$ as the resonant modes $\mathbf{k}_1$ and $\mathbf{k}_2$) no longer satisfy the perfect Bragg resonance condition and therefore the population transfer during the π-pulse is not 100 % efficient (see Supplementary Information). As these components have unequal absolute momenta, their amplitudes accumulate a nonzero relative phase due to phase dispersion during the free propagation. The accrued relative phase results in interference fringes upon the recombination on the beamsplitter, with an approximate period of $\Delta k \simeq \pi m/(\hbar k_r \Delta t_{\text{free}}) \simeq 0.1|\mathbf{k}_0|$.

Due to the indistinguishability of the paths of the Bragg-resonant modes $\mathbf{k}_1$ and $\mathbf{k}_2$ through the beam-splitter and the resulting destructive quantum interference, a measurement of coincidence counts between the atomic populations in these modes will reveal a suppression compared to the background level. To reveal the full structure of the HOM dip, including the background level where no quantum interference occurs, we must introduce path distinguishability between the $\mathbf{k}_1$ and $\mathbf{k}_2$ modes. One way to achieve this, which would be in a direct analogy with shifting the beam splitter in the optical HOM scheme, is to change the Bragg-pulse resonance condition from the $(\mathbf{k}_1, \mathbf{k}_2)$ pair to $(\mathbf{k}_1, \mathbf{k}_2 + \hat{\mathbf{e}}_x \delta k)$, where $\hat{\mathbf{e}}_x$ is the unit vector in the x-direction. The approach to the background coincidence rate between the populations in the $\mathbf{k}_1$ and $\mathbf{k}_2$ modes would then correspond to performing the same experiment for increasingly large displacements δk. Taking into account that acquiring statistically significant results for each δk requires repeated runs of the experiment (typically thousands), this measurement protocol could potentially pose a significant practical challenge due to the very large total number of experimental runs required.

2.3 Results and Discussion

To overcome this challenge, we propose an alternative measurement protocol which can reveal the full structure of the HOM dip from just one Bragg-resonance condition, requiring only one set of experimental runs. The protocol takes advantage of the broadband, multimode nature of the scattering halo and the fact that the original Bragg pulse couples not only the targeted momentum modes $\mathbf{k}_1$ and $\mathbf{k}_2$, but also many other pairs of modes which follow distinguishable paths through the beam-splitter. One such pair, $\mathbf{k}_3 = (k_x, k_y, k_z) = k_r(\cos(\theta), \sin(\theta), 0)$ and $\mathbf{k}_4 = -\mathbf{k}_3$, located on the halo peak, is shown in Fig. 2.3a and corresponds to a rotation by angle θ away from $\mathbf{k}_1$ and $\mathbf{k}_2$. The modes $\mathbf{k}_3$ and $\mathbf{k}_4$ are equivalent to the original pair in the sense of their quantum statistical properties and therefore, these modes can be used for the measurement of the background level of coincidence counts, instead of physically altering the paths of the $\mathbf{k}_1$ and $\mathbf{k}_2$ modes. The angle θ now serves the role of the 'displacement' parameter that scans through the shape of the HOM dip.

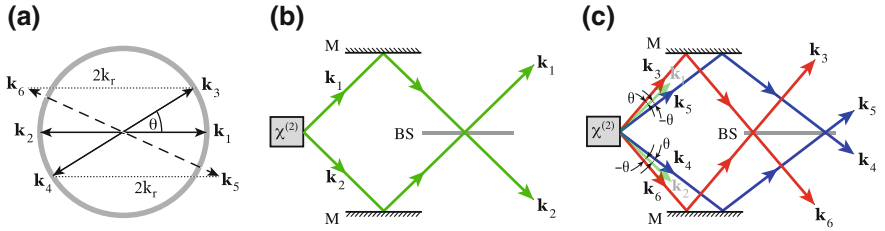

Fig. 2.3 Panel (**a**) shows the schematic of a set of momentum modes affected by the Bragg pulses. The diametrically opposite vectors $\mathbf{k}_1$ and $\mathbf{k}_2 = -\mathbf{k}_1$ show the targeted modes; their amplitude is given by the halo peak radius, $k_r = |\mathbf{k}_1| = |\mathbf{k}_2|$, which is equal to $k_r = 0.95|\mathbf{k}_0|$ in this part of the halo [9]. Also shown are the to-be-measured momentum components $\mathbf{k}_3$ and $\mathbf{k}_4$ corresponding to a rotation by θ away from the targeted modes, which couple, respectively, to $\mathbf{k}_6 = \mathbf{k}_3 - 2\mathbf{k}_1$ and $\mathbf{k}_5 = \mathbf{k}_4 + 2\mathbf{k}_1$ by the same Bragg pulses. Panels (**b**) and (**c**) show a topologically equivalent optical scheme. A $\chi^{(2)}$ nonlinear crystal is optically pumped to produce twin-photons via parametric down-conversion. In (**b**) we depict the archetypal optical HOM setup which corresponds to the case of $\theta = 0$ in the atom-optics scheme. A twin-photon state in modes $\mathbf{k}_1$ and $\mathbf{k}_2$ is first selected from a broadband source, then mixed at the beam-splitter (*BS*) after reflection from the mirror (*M*), and photon coincidence counts are measured between the two symmetric output ports of the interferometer. In (**c**) we depict the optical setup which is equivalent to $\theta > 0$ in the atom-optics proposal. Two twin-photon states in ($\mathbf{k}_3$, $\mathbf{k}_4$) and in ($\mathbf{k}_5$, $\mathbf{k}_6$) are selected from the broadband source; the asymmetry of the pairs about the optical axis of the interferometer means that the correlated photons from the respective pairs will arrive at the beam-splitter at spatially separate locations and will mix with photons from the other pair, which introduces distinguishability between the paths through the interferometer

A topologically equivalent optical scheme is shown in Fig. 2.3b, c, which is in turn similar to the one analysed in Ref. [25] using a broadband source of angle-separated pair-photons and directionally asymmetric apertures.

In the proposed protocol, detection (after the final Bragg pulse) of atom coincidences at the pair of originally correlated momenta $\mathbf{k}_3$ and $\mathbf{k}_4$ corresponds to both paths being separately *reflected* on the beamsplitter (see Fig. 2.3c). Apart from this outcome, we need to take into account the coincidences between the respective Bragg-partner momenta, $\mathbf{k}_6$ and $\mathbf{k}_5$ (separated, respectively, from $\mathbf{k}_3$ and $\mathbf{k}_4$ by the same difference $2k_r$ as $\mathbf{k}_1$ from $\mathbf{k}_2$). Coincidences at $\mathbf{k}_6$ and $\mathbf{k}_5$ correspond to atoms of the originally correlated momenta $\mathbf{k}_3$ and $\mathbf{k}_4$ being both *transmitted* through the beam splitter (see Fig. 2.3c). Finally, in order to take into account all possible channels contributing to coincidence counts between the two arms of the interferometer, we need to measure coincidences between $\mathbf{k}_3$ and $\mathbf{k}_6$, as well as between $\mathbf{k}_4$ and $\mathbf{k}_5$. This ensures that the total detected flux at the output ports of the beam splitter matches the total input flux. In addition to this, we normalise the bare coincidence counts to the product of single-detector count rates, i.e., the product of the average number of atoms in the two output arms of the interferometer. We use the normalised correlation function as the total population in the four relevant modes varies as the angle θ is increased, implying that the raw coincidence rates are not a suitable quantity to compare at different angles.

With this measurement protocol in mind, we quantify the HOM effect using the normalised second-order correlation function $\overline{g}^{(2)}_{\mathrm{RL}}(t) = \langle :\hat{N}_{\mathrm{R}}(t)\hat{N}_{\mathrm{L}}(t):\rangle / \langle \hat{N}_{\mathrm{R}}(t)\rangle \langle \hat{N}_{\mathrm{L}}(t)\rangle$ after the $\pi/2$-pulse concludes at $t = t_4$. Here, $\langle \hat{N}_{\mathrm{R}}\rangle \equiv \langle \hat{N}_3\rangle + \langle \hat{N}_5\rangle$ and $\langle \hat{N}_{\mathrm{L}}\rangle \equiv \langle \hat{N}_4\rangle + \langle \hat{N}_6\rangle$ correspond to the number of atoms detected, respectively, on the two (right and left) output ports of the beam splitter, with the detection bins centred around the four momenta of interest $\mathbf{k}_i$ ($i = 3$, 4, 5, and 6), for any given angle θ [see Fig. 2.2e]. More specifically, $\hat{N}_i(t) = \int_{\mathcal{V}(\mathbf{k}_i)} d^3\mathbf{k}\, \hat{n}(\mathbf{k}, t)$ is the atom number operator in the integration volume $\mathcal{V}(\mathbf{k}_i)$ centred around $\mathbf{k}_i$, where $\hat{n}(\mathbf{k}, t) = \hat{a}^\dagger(\mathbf{k}, t)\hat{a}(\mathbf{k}, t)$ is the momentum-space density operator, with $\hat{a}^\dagger(\mathbf{k}, t)$ and $\hat{a}(\mathbf{k}, t)$ the corresponding creation and annihilation operators (the Fourier components of the field operators $\hat{\delta}^\dagger(\mathbf{r}, t)$ and $\hat{\delta}(\mathbf{r}, t)$, see Methods). The double-colon notation in $\langle :\hat{N}_{\mathrm{R}}(t)\hat{N}_{\mathrm{L}}(t):\rangle$ indicates normal ordering of the creation and annihilation operators.

The integrated form of the second-order correlation function, which quantifies the correlations in terms of atom number coincidences in detection bins of certain size rather than in terms of local density-density correlations, accounts for limitations in the experimental detector resolution, in addition to improving the signal-to-noise ratio which is typically low due to the relatively low density of the scattering halo; in typical condensate collision experiments and in our simulations, the low density translates to a typical halo-mode occupation of ~0.1. We choose $\mathcal{V}(\mathbf{k}_i)$ to be a rectangular box with dimensions corresponding to the rms width of the initial momentum distribution of the trapped condensate, which is a reasonable approximation to the mode (or coherence) volume in the scattering halo [8, 22].

The second-order correlation function $\overline{g}^{(2)}_{\mathrm{RL}}(t_4)$, quantifying the HOM effect as a function of the path-distinquishability angle θ, is shown in Fig. 2.4. For $\theta = 0$, where $\mathbf{k}_{3(4)} = \mathbf{k}_{1(2)}$, we observe maximum suppression of coincidence counts relative to the background level due to the indistinguishability of the paths. As we increase $|\theta| > 0$,

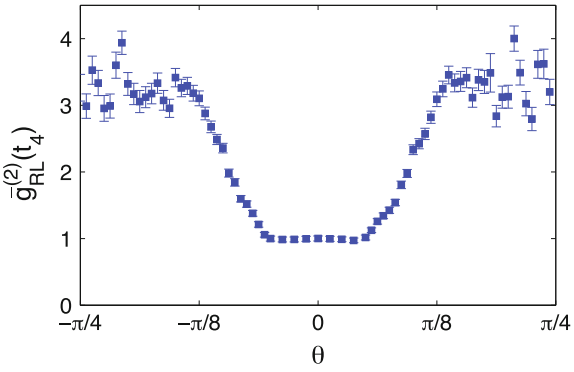

Fig. 2.4 Normalised atom-atom correlation function $\overline{g}^{(2)}_{\mathrm{RL}}(t_4)$ between the two arms of the interferometer, characterising the HOM effect as a function of the path-distinguishability angle θ. Error bars denote sampling error from ~30,000 stochastic simulations (see Methods). The atom counting bins are *rectangular boxes* with sides $\delta k_x = 0.01k_0$ and $\delta k_{y,z} = 0.19k_0$ which approximate the widths of the momentum distribution of the initial trapped BEC

we no longer mix $\mathbf{k}_3$ and $\mathbf{k}_4$ as a pair and their paths through the beam-splitter become distinguishable; the path interference is lost, and we observe an increase in the magnitude of the correlation function to the background level. We quantify the visibility of the HOM dip via $V = 1 - \min\{\overline{g}^{(2)}_{\mathrm{RL}}(t_4)\}/\max\{\overline{g}^{(2)}_{\mathrm{RL}}(t_4)\}$, where $\min\{\overline{g}^{(2)}_{\mathrm{RL}}(t_4)\}$ occurs for $\theta = 0$ and $\max\{\overline{g}^{(2)}_{\mathrm{RL}}(t_4)\}$ for sufficiently large θ such that momenta $\mathbf{k}_{5,6}$ lie outside the scattering halo. Due to the oscillatory nature of the wings (see below) we take $\max\{\overline{g}^{(2)}_{\mathrm{RL}}(t_4)\}$ to correspond to the mean of $\overline{g}^{(2)}_{\mathrm{RL}}(t_4)$ for $\theta \gtrsim \pi/8$. Using this definition we measure a visibility of $V \simeq 0.69 \pm 0.09$, where the uncertainty of ± 0.09 corresponds to taking into account the full fluctuations of $g^{(2)}_{\mathrm{RL}}(t_4)$ about the mean in the wings rather than fitting the oscillations (see Supplementary Information). The visibility larger than 0.5 is consistent with the nonclassical effect of violation of Cauchy–Schwarz inequality with matter waves, observed recently in condensate collision experiments [11]. The exact relationship between the visibility and the Cauchy–Schwarz inequality is discussed further in the Supplementary Information, as are simple (approximate) analytic estimates of the magnitude of the HOM dip visibility.

The broadband, multimode nature of the scattering halo implies that the range of the path-length difference over which the HOM effect can be observed is determined by the spectral width of the density profile of the scattering halo. Therefore the width of the HOM dip is related to the width of the halo density. This is similar to the situation analysed in Ref. [25] using pair-photons from a broadband parametric down-converter. The angular width of the HOM dip extracted from Fig. 2.4 is approximately $w_{\mathrm{HOM}} \simeq 0.61$ radians, which is indeed close to the width (full width at half maximum) of the scattering halo in the relevant direction, $w_{\mathrm{halo}} \simeq 0.69$ radians (see also Supplementary Information for simple analytic estimates). The same multimode nature of the scattering halo contributes to the oscillatory behaviour in the wings of the HOM dip profile: here we mix halo modes with unequal absolute momenta and the resulting phase dispersion from free-propagation leads to oscillations similar to those observed with two-color photons [25].

We emphasise that the input state in our matter-wave HOM interferometer is subtly different from the idealised twin-Fock state $|1, 1\rangle$ used in the simplest analytic descriptions of the optical HOM effect. This idealised state stems from treating the process of spontaneous optical parametric down-conversion (SPDC) in the weak-gain regime. We illustrate this approximation by considering a two-mode toy model of the process, which in the undepleted pump approximation is described by the Hamiltonian $\hat{H} = \hbar g(\hat{a}_1^\dagger \hat{a}_2^\dagger + h.c.)$ that produces perfectly correlated photons in the $\hat{a}_1$ and $\hat{a}_2$ modes, where $g > 0$ is a gain coefficient related to the quadratic nonlinearity of the medium and the amplitude of the coherent pump beam. (In the context of condensate collisions, the coupling g corresponds to $g = U\rho_0(0)/\hbar$ at the same level of 'undepleted pump' approximation [8, 22]; see Methods for the definitions of U and ρ_0.) The full output state of the SPDC process in the Schrödinger picture is given by $|\psi\rangle = \sqrt{1-\alpha^2}\sum_{n=0}^{\infty} \alpha^n |n, n\rangle$, where $\alpha = \tanh(gt)$ and t is the interaction time [26]. In the weak-gain regime, corresponding to $\alpha \simeq gt \ll 1$, this state is well approximated by $|\psi\rangle \propto |0, 0\rangle + \alpha|1, 1\rangle$, i.e., by truncating the expansion of $|\psi\rangle$

and neglecting the contribution of the $|2, 2\rangle$ and higher-n components. This regime corresponds to mode populations being much smaller than one, $\langle\hat{n}\rangle = \langle\hat{a}^{\dagger}_{1(2)}\hat{a}_{1(2)}\rangle = \sinh^2(gt) \simeq (gt)^2 \simeq \alpha^2 \ll 1$. The truncated state itself is qualitatively identical to the idealised state $|1, 1\rangle$ as an input to the HOM interferometer: both result in a HOM dip minimum of $\bar{g}^{(2)}_{\mathrm{RL}} = 0$ and $\bar{g}^{(2)}_{\mathrm{RL}} \simeq 1/2\langle\hat{n}\rangle$ in the wings, with the resulting maximum visibility of $V = 1$. If, on the other hand, the contribution of the $|2, 2\rangle$ and higher-n components is not negligible (which is the case, for example, of $\langle\hat{n}\rangle \simeq 0.1$) then the raw coincidence counts at the HOM dip and the respective normalised correlation function no longer equal to zero; in fact, the full SPDC state for arbitrary $\alpha < 1$ leads to a HOM dip minimum of $\bar{g}^{(2)}_{\mathrm{RL}} = 1$ and $\bar{g}^{(2)}_{\mathrm{RL}} = 2 + 1/2\langle\hat{n}\rangle$ in the wings, which in turn results in a reduced visibility of $V = 1 - 1/(2 + 1/2\langle\hat{n}\rangle)$.

The process of four-wave mixing of matter-waves gives rise to an output state analogous to the above SPDC state for each pair of correlated modes (see, e.g., [8, 22] and Supplementary Information). Indeed, the fraction of atoms converted from the source BEC to all scattering modes is typically less than 5 %, which justifies the use of the undepleted pump approximation. The typical occupation numbers of the scattered modes are, however, beyond the extreme of a very weak gain. In our simulations, the mode occupation on the scattering halo is on the order of 0.1 and therefore, even in the simplified analytical treatment of the process, the output state of any given pair of correlated modes cannot be approximated by the truncated state $|0, 0\rangle + \alpha|1, 1\rangle$ or indeed the idealised twin-Fock state $|1, 1\rangle$.

At the basic level, our proposal only relies on the existence of the aforementioned pair-correlations between scattered atoms, with the strength of the correlations affecting the visibility of the HOM dip. For a sufficiently homogeneous source BEC [22, 27], the correlations and thus the visibility V effectively depend only on the average mode population $\langle\hat{n}\rangle$ in the scattering halo, with a scaling of V on $\langle\hat{n}\rangle$ given by $V = 1 - 1/(2 + 1/2\langle\hat{n}\rangle)$ by our analytic model. Dependence of $\langle\hat{n}\rangle$ on system parameters such as the total number of atoms in the initial BEC, trap frequencies, and collision duration is well understood both theoretically and experimentally [8–11], and each can be sufficiently controlled such that a suitable mode population of $\langle\hat{n}\rangle \lesssim 1$ can, in principle, be targeted. There lies, however, a need for optimisation: very small populations are preferred for higher visibility, but they inevitably lead to a low signal-to-noise, hence requiring a potentially very large number of experimental runs for acquiring statistically significant data. Large occupations, on the other hand, lead to higher signal-to-noise, but also to a degradation of the visibility towards the nonclassical threshold of $V = 0.5$. The mode population of $\sim$0.1 resulting from our numerical simulations appears to be a reasonable compromise; following the scaling of the visibility with $\langle\hat{n}\rangle$ predicted by the simple analytic model, it appears that one could safely increase the population to $\sim$0.2 before a nonclassical threshold is reached to within a typical uncertainty of $\sim$13 % (as per quoted value of $V \simeq 0.69 \pm 0.09$) obtained through our simulations.

The proposal is also robust to other experimental considerations such as the implementation of the Bragg pulses; e.g., one may use square Bragg pulses rather than Gaussians. Furthermore, experimental control of the Bragg pulses is sufficiently

accurate to avoid any degradation of the dip visibility. Modifying the relative timing of the π and $\pi/2$ pulses by few percent in our simulations does not explicitly affect the dip visibility, rather only the period of the oscillations in the wings of $\overline{g}^{(2)}_{\mathrm{RL}}(t_4)$. This may lead to a systematic change in the calculated dip visibility, however, this is overwhelmed by the uncertainty of 13 % which accounts for the fluctuations of $\overline{g}^{(2)}_{\mathrm{RL}}(t_4)$ about the mean.

Importantly, we expect that the fundamentally new aspects of the matter-wave setup, namely the multimode nature of the scattering halo and the differences from the archetypical HOM input state of $|1, 1\rangle$, as well as the specific measurement protocol we have proposed for dealing with these new aspects, are broadly applicable to other related matter-wave setups that generate pair-correlated atoms. These include molecular dissociation [19], an elongated BEC in a parametrically shaken trap [14], or degenerate four-wave mixing in an optical lattice [28, 29]. In the present work, we focus on condensate collisions only due to the accurate characterisation, both experimental and theoretical, of the atom-atom correlations, including in a variety of collision geometries [7–11].

2.4 Conclusion

In summary, we have shown that an atom-optics analogue of the Hong–Ou–Mandel effect can be realised using colliding condensates and a sequence of Bragg pulses. The HOM dip visibility greater than 50 % implies that the atom-atom correlations in this process cannot be described by classical stochastic random variables. Generation and detection of such quantum correlations in matter waves can serve as precursors to stronger tests of quantum mechanics such as those implied by a Bell inequality violation and the Einstein–Podolsky–Rosen paradox [30]. In particular, the experimental demonstration of the atom-optics HOM effect would serve as a suitable starting point to experimentally demonstrate a violation of a Bell inequality using an atom-optics adaptation of the Rarity–Tapster setup [17]. In this setup, one would tune the Bragg pulses as to realise two separate HOM-interferometer arms, enabling to mix *two* angle-resolved pairs of momentum modes from the collisional halo, such as $(\mathbf{k}, \mathbf{q})$ and $(-\mathbf{k}, -\mathbf{q})$, which would then form the basis of a Bell state $|\Psi\rangle = \frac{1}{\sqrt{2}}(|\mathbf{k}, -\mathbf{k}\rangle + |\mathbf{q}, -\mathbf{q}\rangle)$ [31].

References

1. Hong, C.K., Ou, Z.Y., Mandel, L.: Measurement of subpicosecond time intervals between two photons by interference. Phys. Rev. Lett. **59**, 2044–2046 (1987)
2. Ou, Z.Y., Mandel, L.: Violation of Bell's inequality and classical probability in a two-photon correlation experiment. Phys. Rev. Lett. **61**, 50–53 (1988)
3. Knill, E., Laflamme, R., Milburn, G.J.: A scheme for efficient quantum computation with linear optics. Nature **409**, 46 (2001)

4. Kok, P., Lee, H., Dowling, J.P.: Creation of large-photon-number path entanglement conditioned on photodetection. Phys. Rev. A **65**, 052104 (2002)
5. Duan, L.-M., Monroe, C.: Colloquium: quantum networks with trapped ions. Rev. Mod. Phys. **82**, 1209–1224 (2010)
6. Lang, C., et al.: Correlations, indistinguishability and entanglement in Hong-Ou-Mandel experiments at microwave frequencies. Nat. Phys. **9**, 345–348 (2013)
7. Perrin, A., et al.: Observation of atom pairs in spontaneous four-wave mixing of two colliding Bose-Einstein condensates. Phys. Rev. Lett. **99**, 150405 (2007)
8. Perrin, A., et al.: Atomic four-wave mixing via condensate collisions. New J. Phys. **10**, 045021 (2008)
9. Krachmalnicoff, V., et al.: Spontaneous four-wave mixing of de Broglie waves: beyond optics. Phys. Rev. Lett. **104**, 150402 (2010)
10. Jaskula, J.-C., et al.: Sub-Poissonian number differences in four-wave mixing of matter waves. Phys. Rev. Lett. **105**, 190402 (2010)
11. Kheruntsyan, K.V., et al.: Violation of the Cauchy-Schwarz inequality with matter waves. Phys. Rev. Lett. **108**, 260401 (2012)
12. Kozuma, M., et al.: Coherent splitting of Bose-Einstein condensed atoms with optically induced Bragg diffraction. Phys. Rev. Lett. **82**, 871–875 (1999)
13. Meystre, P.: Atom Optics. Springer, New York (2001)
14. Bücker, R., et al.: Twin-atom beams. Nat. Phys. **7**, 608 (2011)
15. Lücke, B., et al.: Twin matter waves for interferometry beyond the classical limit. Science **334**, 773 (2011)
16. Gross, C., et al.: Atomic homodyne detection of continuous-variable entangled twin-atom states. Nature **480**, 219 (2011)
17. Rarity, J.G., Tapster, P.R.: Experimental violation of Bell's inequality based on phase and momentum. Phys. Rev. Lett. **64**, 2495–2498 (1990)
18. Norrie, A.A., Ballagh, R.J., Gardiner, C.W.: Quantum turbulence and correlations in Bose-Einstein condensate collisions. Phys. Rev. A **73**, 043617 (2006)
19. Savage, C.M., Schwenn, P.E., Kheruntsyan, K.V.: First-principles quantum simulations of dissociation of molecular condensates: atom correlations in momentum space. Phys. Rev. A **74**, 033620 (2006)
20. Deuar, P., Drummond, P.D.: Correlations in a BEC collision: first-principles quantum dynamics with 150 000 atoms. Phys. Rev. Lett. **98**, 120402 (2007)
21. Mølmer, K., et al.: Hanbury Brown and Twiss correlations in atoms scattered from colliding condensates. Phys. Rev. A **77**, 033601 (2008)
22. Ogren, M., Kheruntsyan, K.V.: Atom-atom correlations in colliding Bose-Einstein condensates. Phys. Rev. A. **79**, 021606 (2009)
23. Deuar, P., Chwedeńczuk, J., Trippenbach, M., Ziń, P.: Bogoliubov dynamics of condensate collisions using the positive-*P* representation. Phys. Rev. A **83**, 063625 (2011)
24. Batelaan, H.: The Kapitza-Dirac effect. Contemp. Phys. **41**, 369–381 (2000)
25. Rarity, J.G., Tapster, P.R.: Two-color photons and nonlocality in fourth-order interference. Phys. Rev. A **41**, 5139–5146 (1990)
26. Braunstein, S.L., van Loock, P.: Quantum information with continuous variables. Rev. Mod. Phys. **77**, 513–577 (2005)
27. Ögren, M., Kheruntsyan, K.V.: Role of spatial inhomogeneity in dissociation of trapped molecular condensates. Phys. Rev. A **82**, 013641 (2010)
28. Hilligsøe, K.M., Mølmer, K.: Phase-matched four wave mixing and quantum beam splitting of matter waves in a periodic potential. Phys. Rev. A **71**, 041602 (2005)
29. Bonneau, M., et al.: Tunable source of correlated atom beams. Phys. Rev. A **87**, 061603 (2013)
30. Kofler, J., et al.: Einstein-Podolsky-Rosen correlations from colliding Bose-Einstein condensates. Phys. Rev. A **86**, 032115 (2012)
31. Lewis-Swan, R.J., Kheruntsyan, K.V.: to be published (see also the Book of Abstracts of ICAP 2012 – The 23rd International Conference on Atomic Physics, 23–27 July 2012, Ecole Polytechnique, Palaiseau, France)

http://www.springer.com/978-3-319-41047-0

Ultracold Atoms for Foundational Tests of Quantum Mechanics

Lewis-Swan, R.J.

2016, XVI, 156 p. 35 illus., 14 illus. in color., Hardcover
ISBN: 978-3-319-41047-0